Motions in Cores

(1) outflows
- more than half of low-mass cores with stars have outflows

(2) rotation
- present at a low level in some objects
- not dynamically important (not important to energy balance)

(3) infall ("the holy grail")
- various pieces of indirect evidence
- most claims to detect infall have been shot down later

(4) random turbulent motions
- source? $\vec{B}$ fields?

What should a collapsing core look like?

Zhou 1992 ApJ

- use 2 models of protostellar collapse
  (1) Larson-Penston flow (isothermal sphere)
  (2) "inside out" collapse (Shu + coworkers)
- both have spherical symmetry

→ take density, velocity structure as a function of time from the models
→ assume constant temperature T = 10 K
- add microturbulent velocity component to Shu et al. models for core-formation stage (otherwise model predicts thermal line widths)

Emission from CS levels
- level populations from microturbulent radiative transfer
- line profiles from level pops, turbulent + systemic velocity fields
- convolved to simulate observing beam

→ asymmetric lines (blue stronger)
→ degree of absorption + line width increases with J
→ asymmetry + absorption disappear at large impact parameters
→ absorption + line width more prominent at higher resolution

Zhou 1992 ApJ

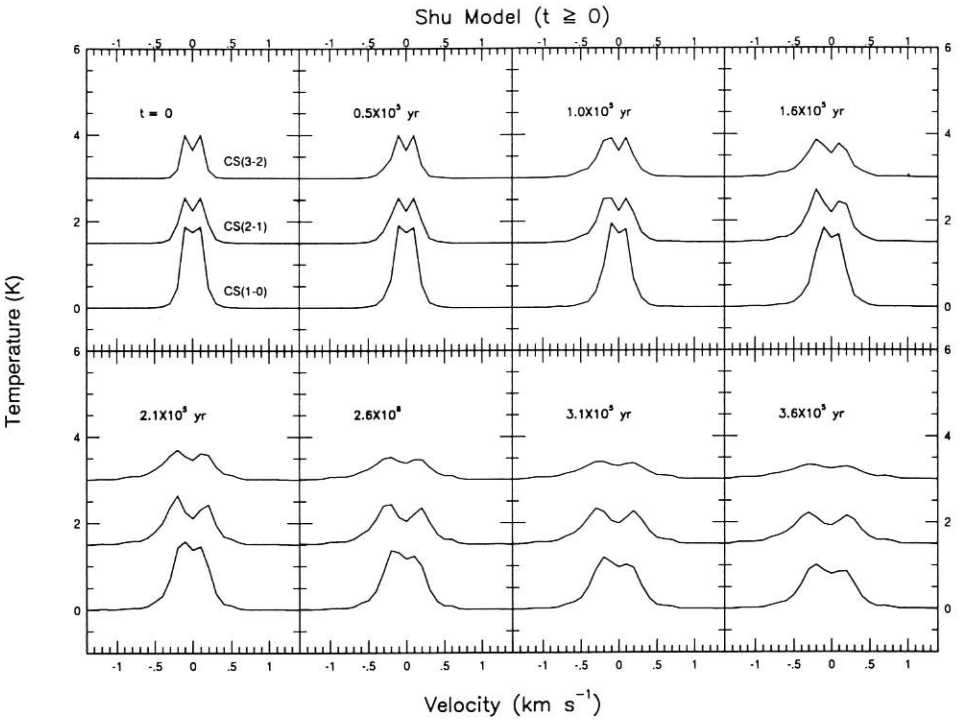

FIG. 3c

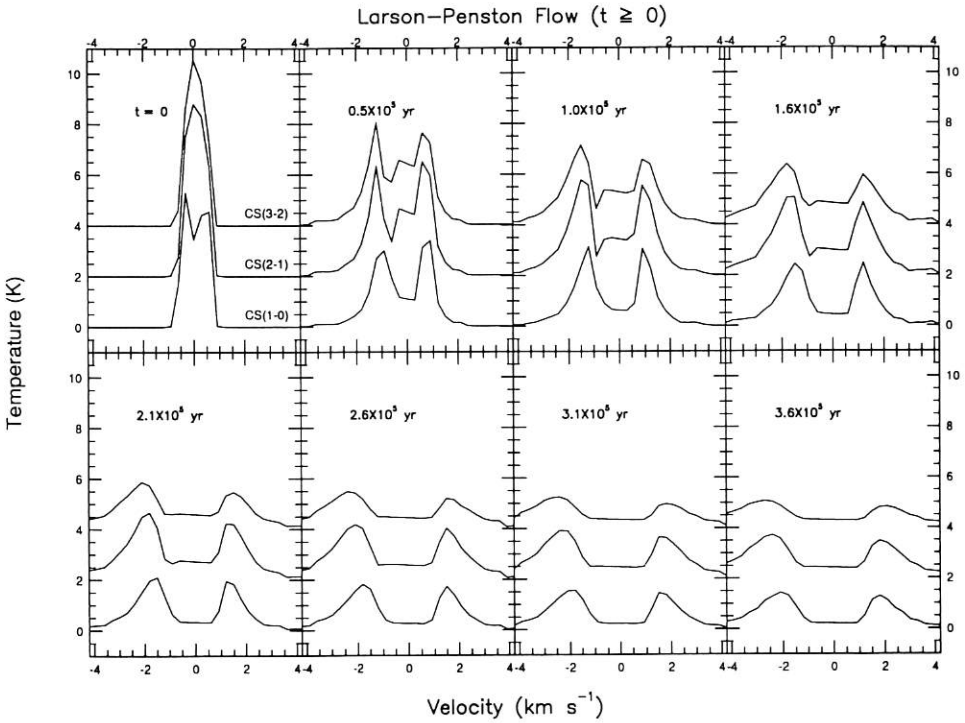

FIG. 3d

(13)

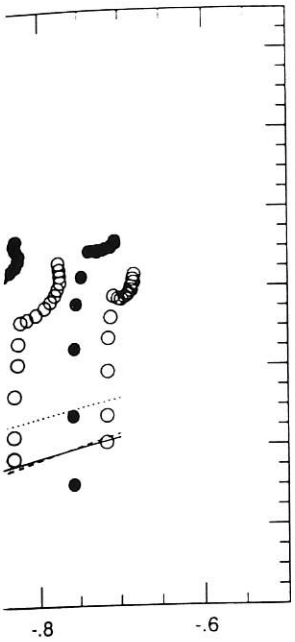

Δv vs. R diagram. The
. R in Myers (1983); the
ound by Fuller (1989) for
ints from the Shu model
ows points from the Shu
and 500 pc (from left to

n the red peak (Fig.
and the line width
ritical density of the
vidth increases with
ıtum number J (Fig.
the surface of dense
rption disappear at
self-absorption and
h higher resolution

to identify collapse
1977). Walker et al.
(2) to conclude the
IRAS 16293−2422,
$J = 2 \rightarrow 1$ and $5 \rightarrow 4$
apping of Menten et

al. (1987) showed that the self-absorption is too narrow and too deep to be explained by infall and the self-absorption is present throughout the core, contradicting property (3). It seems that the emission from IRAS 16293−2422 can be explained better by a rotational model plus a foreground layer of absorbing gas than by infall (Mundy et al. 1986). Unambiguous identification of infall probably involves finding dense cores whose emission has all the properties described above. In addition, detailed knowledge of the temperature and density distribution is required to decipher the velocity field (see Leung & Brown 1977).

To find out if properties (1)–(4) are unique to collapse, we examine the effects of other dynamical processes. First, the line profiles can change as a result of changes in the turbulence field; but turbulence alone should always produce symmetric line profiles rather than the asymmetric profiles expected from infall. Second, outflow can enhance line widths in certain regions of the dense cores; but molecular outflow usually produces line emission that is spatially asymmetric with respect to the cloud center. Thus, the line properties of an infall region are

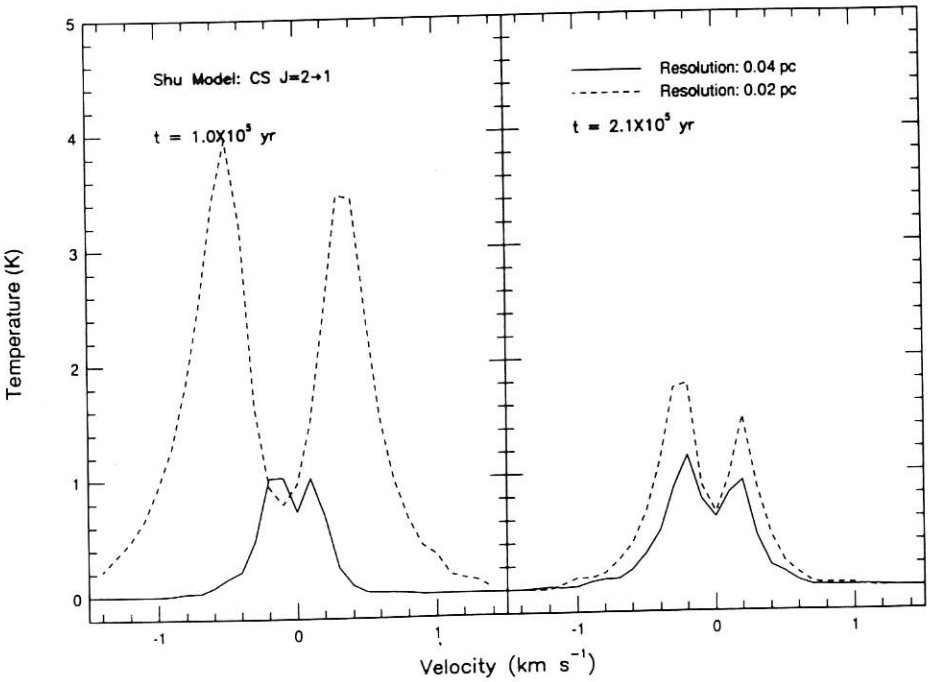

FIG. 9.—The CS $J = 2 \rightarrow 1$ profiles are plotted for two models, each at two different resolutions. The plot shows the variation of line properties with resolutions for collapsing dense cores.

Why should infall produce asymmetric lines?

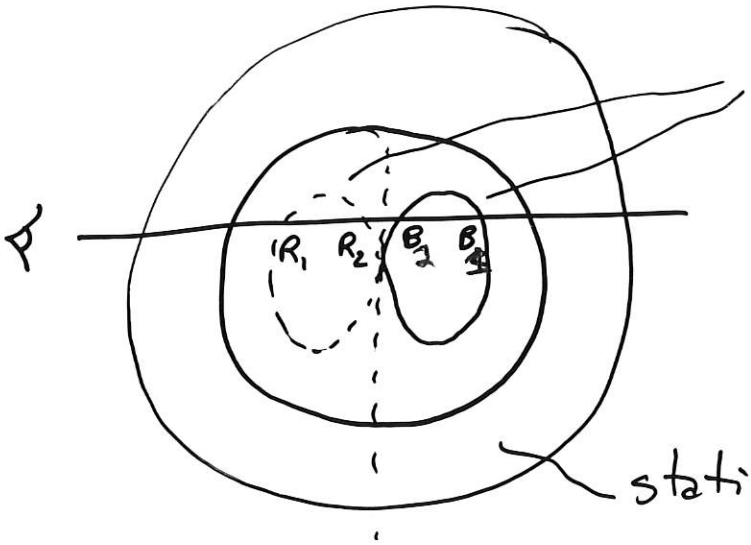

redshifted emission from hemisphere closer to observer
blueshifted " " " farther from "

assume T_1, τ_1 at R_1
T_2, τ_2 at R_2

$$\rightarrow T_{red} = T_2\left(1-e^{-\tau_2}\right)e^{-\tau_1} + T_1\left(1-e^{-\tau_1}\right)$$

similarly

$$T_{blue} = T_1\left(1-e^{-\tau_1}\right)e^{-\tau_2} + T_2\left(1-e^{-\tau_2}\right)$$

$$\therefore T_{blue} - T_{red} = \left(T_2 - T_1\right)\left(1-e^{-\tau_1}\right)\left(1-e^{-\tau_2}\right)$$

$$\rightarrow T_{blue} > T_{red} \text{ iff } T_2 > T_1$$

note $T_{blue} = T_{red}$ if $\tau_1, \tau_2 \ll 1$ $\rightarrow$ optically thin lines symmetric

Gregersen 1997, ApJ, 484, 256

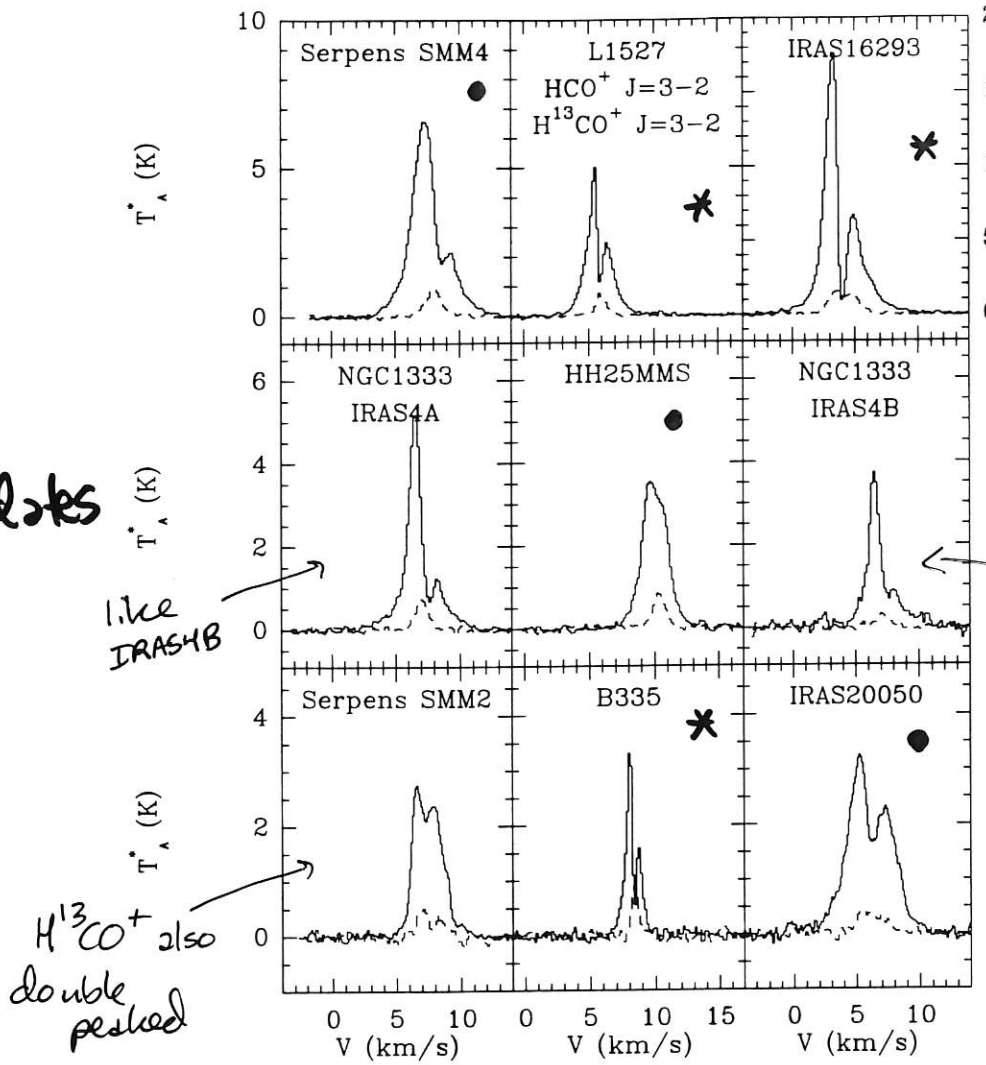

FIG. 1.—HCO^+ and $H^{13}CO^+$ $J = 3–2$ spectra toward the center of nine class 0 sources. These sources all show a blue asymmetry in the HCO^+ $J = 3–2$ line characteristic of collapse. The solid line is the HCO^+ spectrum, and the dashed line is the $H^{13}CO^+$ spectrum. The scale for the spectra of IRAS 16293 is shown on the right-hand side of its panel. The $H^{13}CO^+$ $J = 3–2$ spectrum for HH 25MMS is from the position (0, 6).

- survey of Class 0 sources for infall
- 23 sources $d = 125 - 700$ pc $T_{bol} < 70$ K

HCO^+ J=3-2, 4-3 $H^{13}CO^+$, $HC^{18}O^+$

measure blue/red ratio and skewness of line (over $V_{lsr} = \pm 1.25$ km/s to avoid outflows)

⇒ 6 candidates for infall (3 already known)

Gregersen 1997

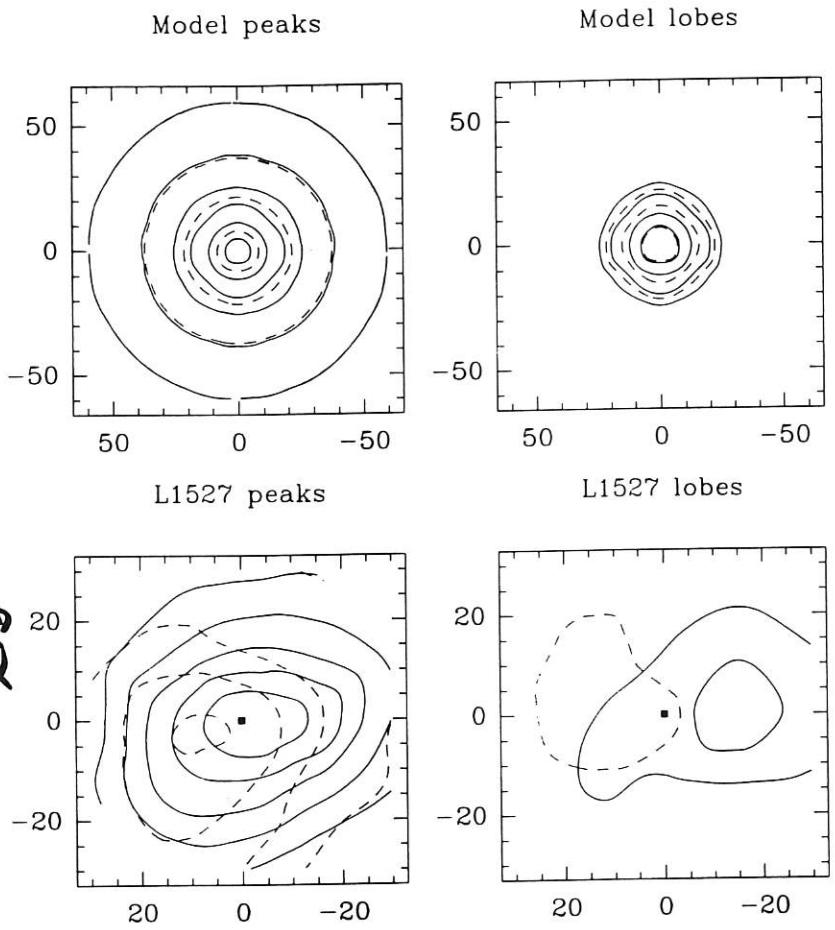

FIG. 13.—The top two plots are integrated intensity maps of the red and blue peaks and the blue and red lobes of the HCO^+ $J = 3–2$ line in a simulation of a collapsing cloud. The velocity intervals are -0.43 to -0.27 km s^{-1} and 0.27–0.43 km s^{-1} for the peaks and -3.09 to -0.43 km s^{-1} and 0.43–3.09 km s^{-1} for the lobes. The contour level spacing is 0.1 then 0.2 K km s^{-1} thereafter. In all plots, the solid contours are the blueshifted peak and the blue line wing and the dashed contours are the redshifted peak and the red line wing, respectively. The middle two plots are integrated intensity maps of the red and blue peaks and the blue and red lobes of the HCO^+ $J = 3–2$ line in L1527. The velocity intervals are 5–5.7 km s^{-1} and 6.1–7 km s^{-1} for the peaks and 2–5 km s^{-1} and 7–10 km s^{-1} for the lobes. The contour level spacing is 1 K km s^{-1} for the peaks and 0.5 K km s^{-1} for the lobes. The black square is the location of the IRAS source. The bottom two plots are integrated intensity maps of the red and blue peaks and the blue and red lobes of the HCO^+ $J = 3–2$ line in NGC 1333 IRAS 4A. The velocity intervals are 4.3–5.09 km s^{-1} and 5.7–6.33 km s^{-1} for the peaks and 2.6–4.3 km s^{-1} and 6.33–8.97 km s^{-1} for the lobes. The contour level spacing is 0.5 K km s^{-1} for the blue peak and blue lobe, 0.25 then 0.5 K km s^{-1} thereafter for the red peak, and 0.1 K km s^{-1} for the red lobe. The two black squares are the location of the submillimeter sources detected by Sandell et al. (1991). The source at (0, 0) is NGC 1333 IRAS 4A, and the source at (22, −23) is NGC 1333 IRAS 4B.

Difficulty → outflows also present → high velocity line wings

Infall → blue & red peak on central source

Outflow → blue & red shifted, on either side of center

Star Formation in Clusters

Testi & Sargent, 1998
ApJ, 508, L91

- many (most?) stars form in clusters
- a complete theory of star formation must predict the stellar **Initial Mass Function (IMF)**
- IMF could result from
  - protostar accretion process
  - fragmentation process
  - competitive accretion in a cluster

→ compare core mass function to IMF

Serpens core
~1500 $M_\odot$
310 pc away
contains a young stellar cluster

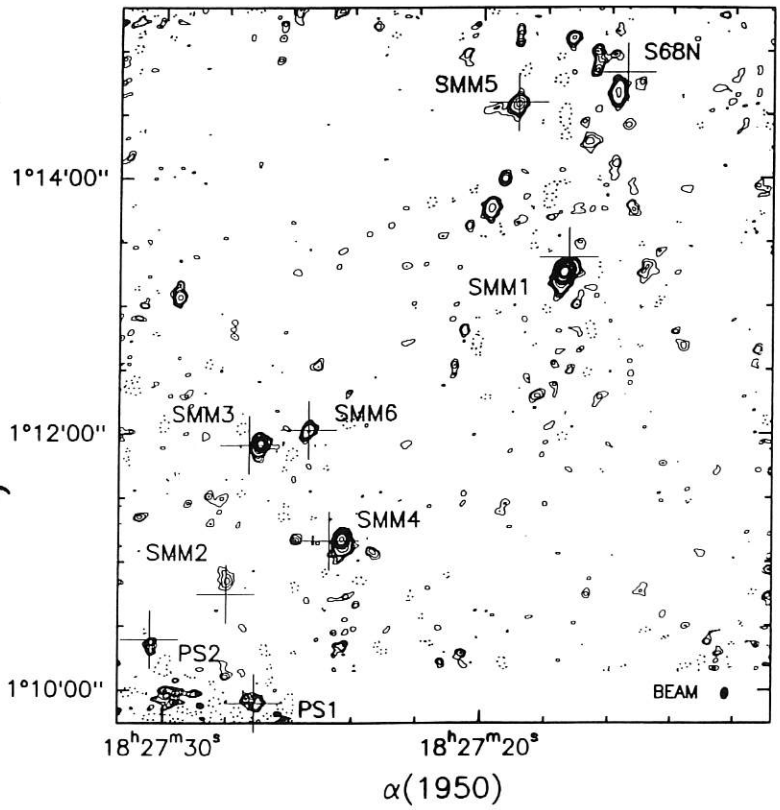

5" ~ 1500 AU

4.5σ limit
~ 4.0 mJy
~ 0.4 $M_\odot$

FIG. 1.—OVRO 3 mm continuum mosaic of the Serpens core. Contour levels are −2.7, 2.7–6.3 by 0.9, 10–42 by 4, and 55–105 by 10 mJy beam^{-1}. The positions of the known submillimeter sources (CED) and far-infrared sources (Hurt & Barsony 1996) are marked by crosses. Note that we detect all the sources already identified and have refined the positional accuracy. In addition, numerous new sources can be seen. The synthesized beam, 5".5 × 4".3 (FWHM), is shown as a filled ellipse in the lower right-hand corner.

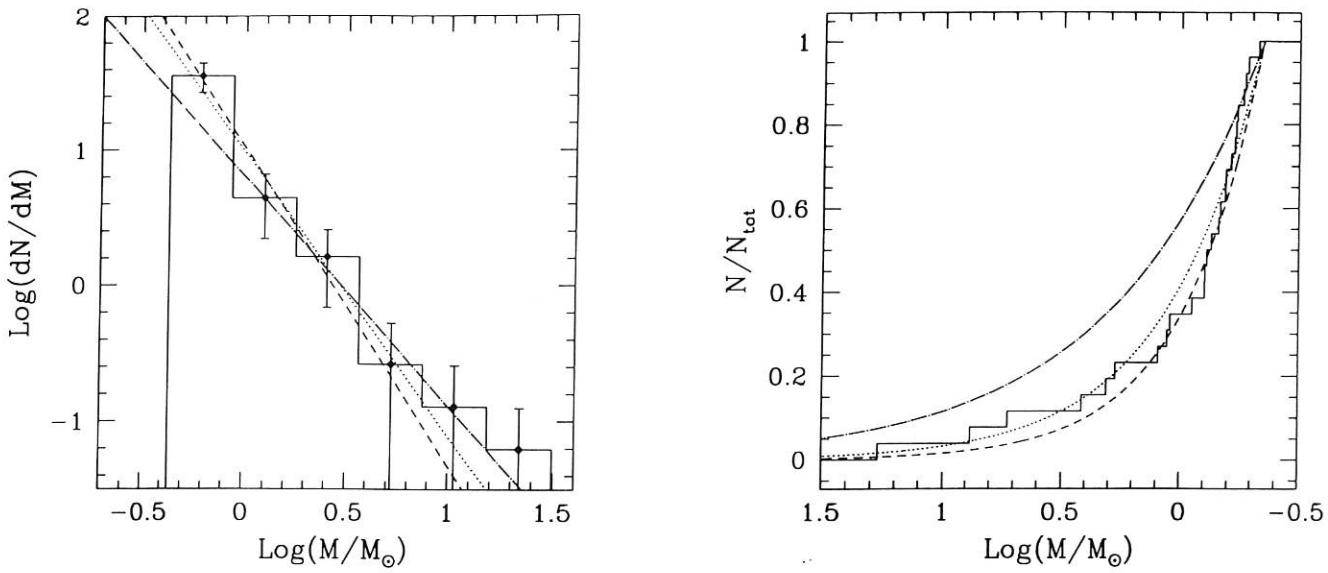

FIG. 3.—*Left panel*: the mass spectrum for the 3 mm continuum sources. The dotted line is the best-fitting power law, $dN/dM \sim M^{-2.1}$; the dashed line represents the Salpeter IMF, $dN/dM \sim M^{-2.35}$; the dot-dashed line is a -1.7 power law. *Right panel*: the normalized cumulative mass distribution. The dotted, dashed, and dot-dashed lines are the same as in the left panel.

$$M = \frac{S_\nu D^2}{K_\nu B_\nu(T)}$$

assume $T = 15$ K

$\kappa = .005 \text{ cm}^2/\text{g} \left[\nu/230\right]^{1.1}$

- 9 previously known + 21 new sources in map
- all sources likely gravitationally bound

→ discard 6 sources with NIR counterparts

mass spectrum $\frac{dN}{dM} \sim M^{-2.1}$

compare to IMF → $M^{-2.35}$ (Salpeter)

gas clumps + clouds → $M^{-1.7}$

→ suggests stellar IMF results from fragmentation rather than accretion

Initial Conditions for Star Formation

Motte et al. 1998, A&A, 336, 150

- wide field mapping of ρ Oph
  d ~ 160 pc
- well surveyed already for protostars, gas cores, etc.

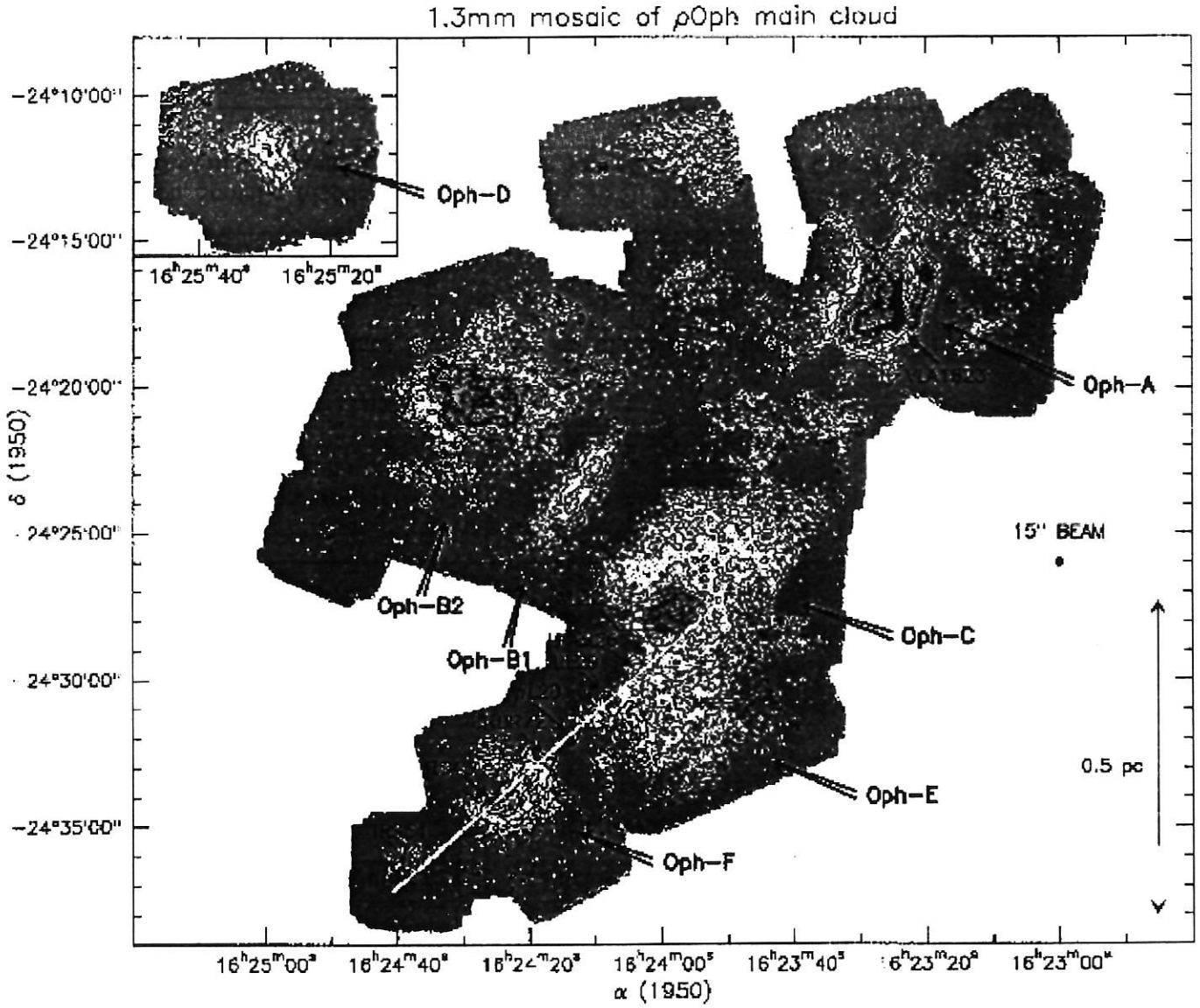

- core has a high star formation efficiency (~20%)
  core size ~1 × 2 pc

Motte et al. 1998

- data complete to $M \sim 0.1\ M_\odot$

→ 58 star-less clumps

(most are likely gravitationally bound)

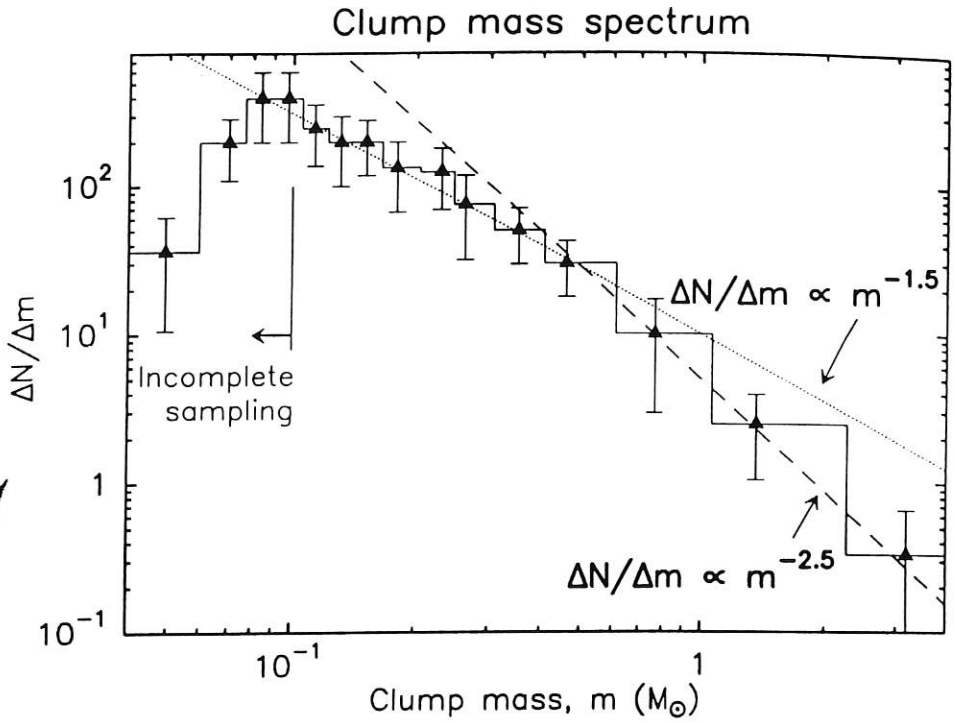

Fig. 5. Frequency distribution of masses for 60 small-scale clumps extracted from the mosaic of Fig. 1 (solid line). The dotted and long-dashed lines show power laws of the form $\Delta N/\Delta m \propto m^{-1.5}$ and $\Delta N/\Delta m \propto m^{-2.5}$, respectively. The error bars correspond to $\sqrt{N}$ counting statistics.

$\frac{dN}{dM} \sim m^{-1.5}$ $\quad 0.1 < M < 0.5\ M_\odot$

$\sim m^{-2.5}$ $\quad 0.5 < M < 3\ M_\odot$

→ clump mass function mimics stellar IMF

[previous molecular line studies of clumps gave a single shallow slope of ~ -1.5]

Double Power Laws

highest mass cloud

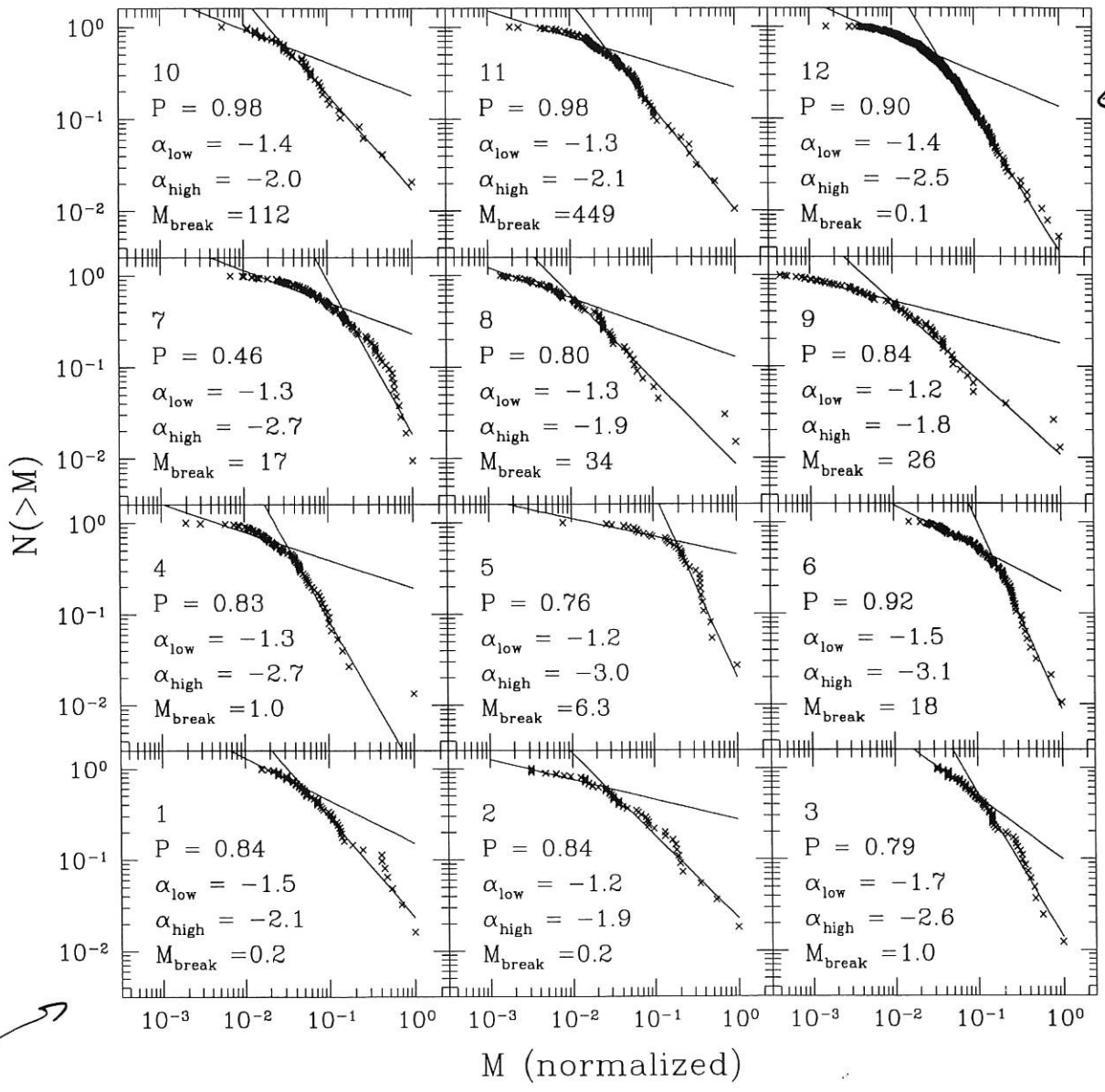

← simulation

lowest mass cloud

Fig. 3.— Cumulative mass functions (*symbols*) for the 12 data sets described in Table 1. Each CMF is fit by a pure double power law (2PL), as described by Equation 6. The panel labels indicate the data set ID from Table 1, goodness-of-fit probability, P, and best-fit parameters, $\alpha_{\rm low}$, $\alpha_{\rm high}$, and $M_{\rm break}$. For visual clarity, the maximum clump mass in each plot has been normalized to unity; the best fit parameters given are for fits to the unnormalized data.

Reid & Wilson 2006, astro-ph 0607095

lognormal: $\frac{\Delta N}{\Delta M} = \frac{1}{A_1\sqrt{2\pi}M} \exp\left[-\frac{(\ln M - A_0)^2}{2A_1^2}\right]$

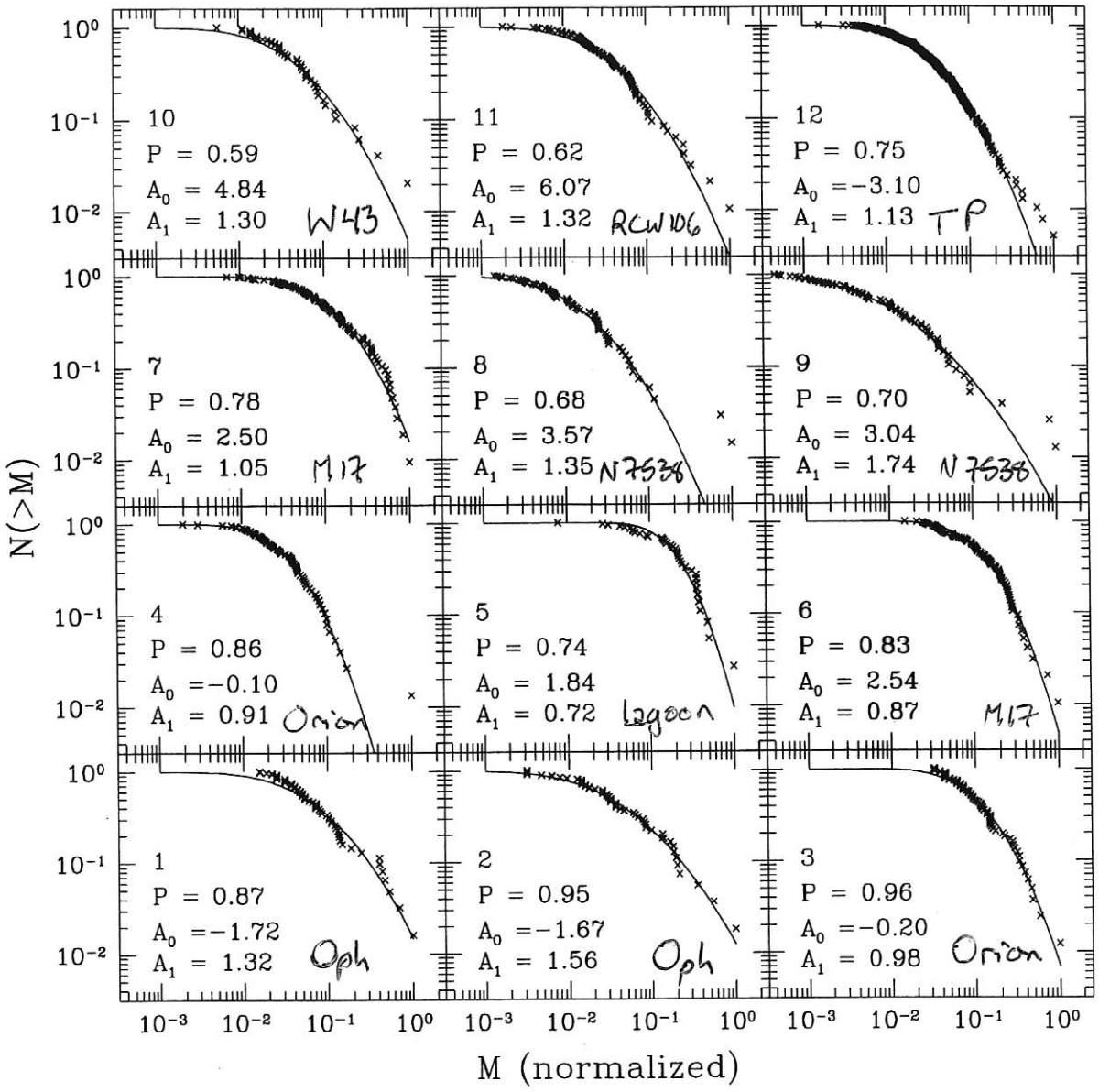

Fig. 6.— Cumulative mass functions (*symbols*) for the 12 data sets described in Table 1. Each CMF is fit by a lognormal clump mass distribution (LOGN), as described by Equation 10. The panel labels indicate the data set ID from Table 1, goodness-of-fit probability, P, and best-fit parameters, A_0 and A_1. For visual clarity, the maximum clump mass in each plot has been normalized to unity; the best fit parameters given are for fits to the unnormalized data.

Reid & Wilson 2006

P. André 2011

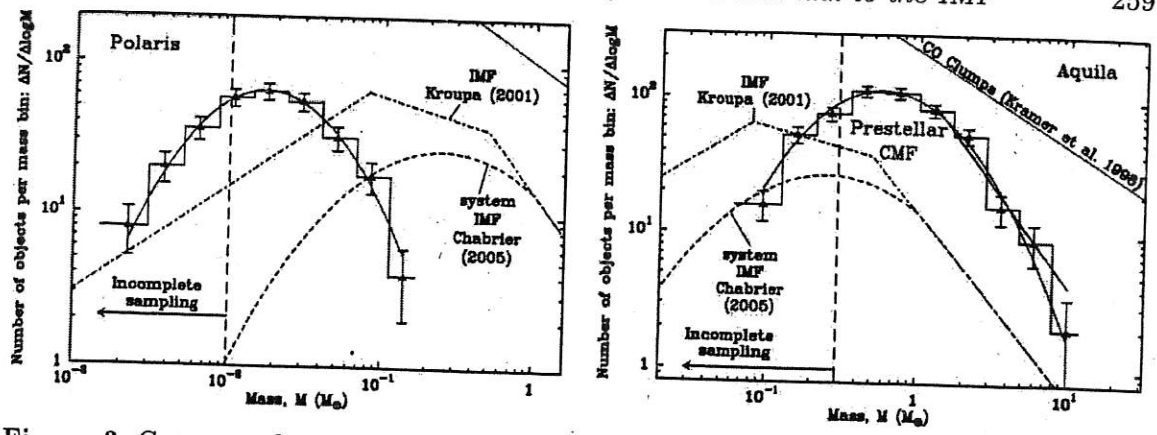

Figure 3. Core mass functions (histograms with error bars) derived from our *Herschel* observations of the Polaris (left) and Aquila (right) regions, which reveal of total of 302 starless cores and 541 candidate prestellar cores, respectively (André *et al.* 2010 and Könyves *et al.* 2010). The IMF of single stars (corrected for binaries – e.g., Kroupa 2001), the IMF of multiple systems (e.g., Chabrier 2005), and the typical mass spectrum of CO clumps (e.g., Kramer *et al.* 1998) are shown for comparison. Log-normal fits to the observed CMFs are superimposed. These fits peak at $\sim 0.02\,M_\odot$ (Polaris) and $\sim 0.6\,M_\odot$ (Aquila), and have standard deviations of ~ 0.41 and ~ 0.43 in $\log_{10} M$, respectively. (For reference, the log-normal part of the Chabrier system IMF peaks at $0.25\,M_\odot$ and has a standard deviation of ~ 0.55 in $\log_{10} M$.)

Herschel Gould Belt survey → nearby (< 500pc) molecular clouds, 70 - 500 μm

Polaris flare - high-latitude translucent, little star formation

Aquila - very active star formation

extremes of sample

Polaris - 300 unbound starless cores
- mass function peaks below IMF

Aquila - 200 protostars + 540 starless cores, of which ~60% gravitationally bound
- comparison to stellar IMF suggests efficiency ~ 25 - 40%

P. André 2011

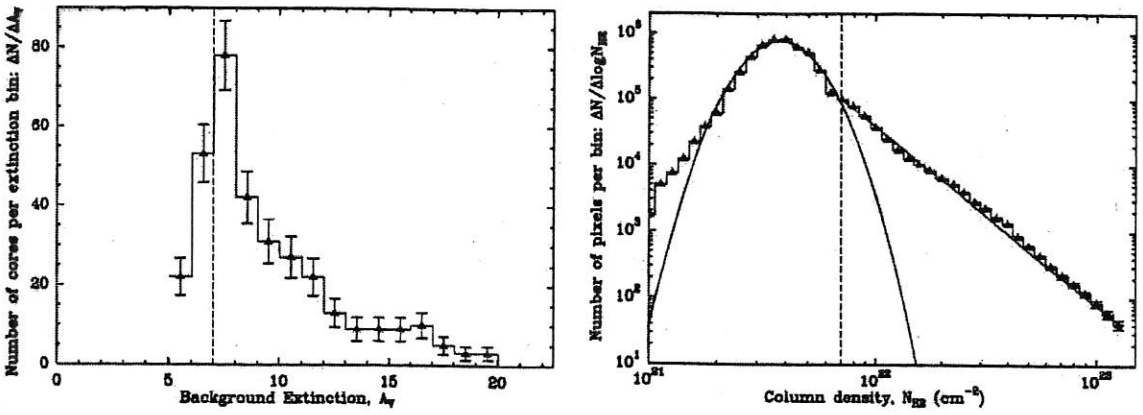

Figure 5. Left: Distribution of background column densities (converted to equivalent extinctions) for the best 341 candidate prestellar cores identified with *Herschel* in the Aquila Rift complex. **Right:** Probability density function of column density in the Aquila complex, based on the column density images derived from our *Herschel* data (cf. Könyves *et al.* 2010). A log-normal fit at low column densities and a power-law fit at high column densities are superimposed. In both panels, the vertical dashed line marks the extinction threshold $A_V^{\rm back} = 7$ (see § 3).

Tight connection between compact cores and filaments in Aquila

→ 90% of bound prestellar cores have background column density $N_{H_2} \gtrsim 7 \times 10^{21}$ cm^{-2} or $A_V \gtrsim 7$ mag

→ threshold for prestellar core formation

Consistent with no bound cores in Polaris

→ background column density too low

Column density PDF shows power law tail → reflects dominant role of gravity above $A_V \sim 7$ mag

→ cores concentrated in gravitationally unstable filaments

Finally, some theory...

(Ballesteros-Paredes et al., PPV, astro-ph 0603357)

- turbulence in molecular clouds is highly supersonic ⇒ Mach numbers ~ 5-20
- this produces large (transient) density enhancements at shocks
  → some clumps and cores may become gravitationally unstable (due to high density)
- turbulence models can predict the clump mass distribution
- but linking this to stellar IMF assumes one star per clump
- other problems/factors are
  - cores merge → changes mass distribution
  - shape of mass spectrum depends on parameters of turbulence
  - competitive accretion ignored
  - stellar feedback ignored
  - changes in EOS may introduce a preferred mass scale

Padoan & Nordlund, 2002, ApJ, 576, 870

L_0 = largest turbulent scale

$\mathcal{M}_0$ = Mach number

n_0 = average density

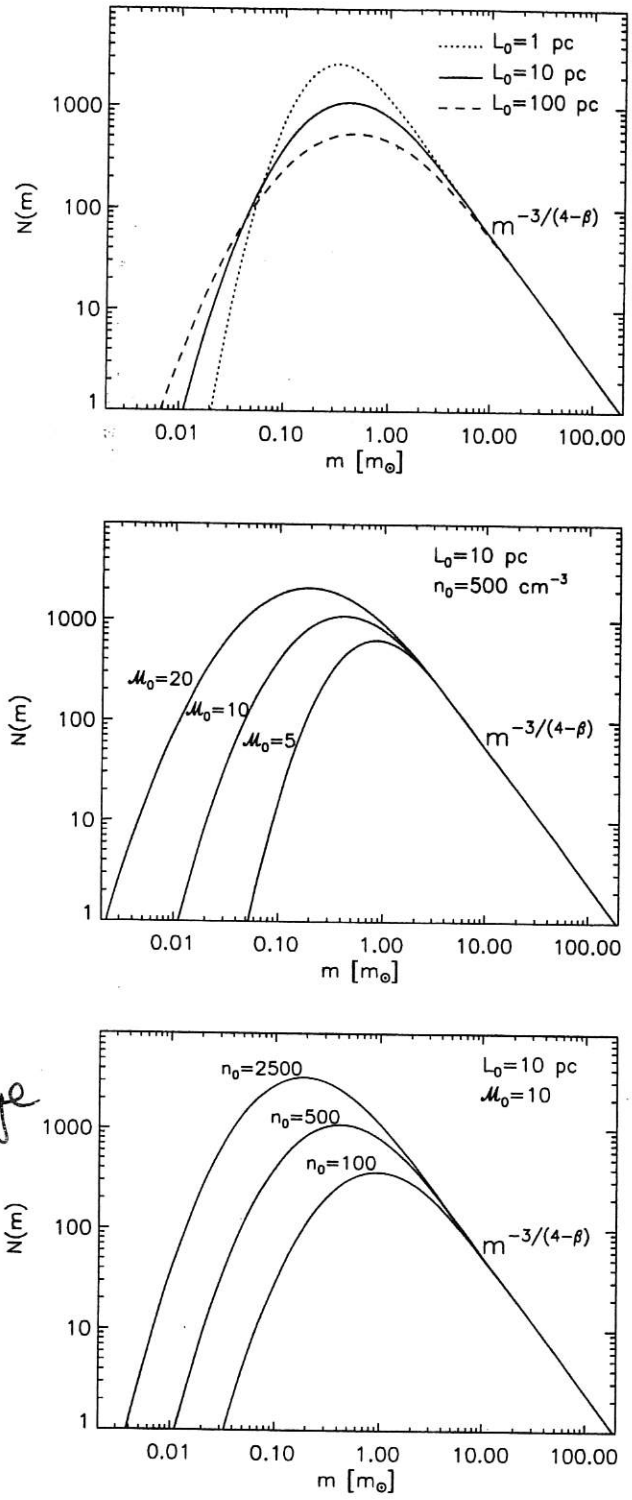

FIG. 1.—Mass distributions of gravitationally unstable cores from eq. (24). *Top:* Mass distribution for different values of the largest turbulent scale L_0, assuming Larson-type relations (for rescaling n_0 and $\mathcal{M}_{A,0}$ with L_0), $T_0 = 10$ K, and $\beta = 1.8$. *Middle:* Mass distribution for different values of $\mathcal{M}_{A,0}$, assuming $n_0 = 500$ cm^{-3}, $T_0 = 10$ K, and $\beta = 1.8$. *Bottom:* Mass distribution for different values of n_0, assuming $\mathcal{M}_{A,0} = 10$, $T_0 = 10$ K, and $\beta = 1.8$. The mass distribution peaks at approximately 0.4 $M_\odot$, for the values $\mathcal{M}_{A,0} = 10$, $n_0 = 500$ cm^{-3}, $T_0 = 10$ K, and $\beta = 1.8$, typical of nearby molecular clouds.

Use
- lognormal distribution of clump densities
- assume power spectrum of turbulence is a power law, and
- typical size of a dense core scales as thickness of postshock gas

⇐ analytical solutions for clump mass function